Drug Design, Development and Therapy

Dovepress
Taylor & Francis Group

Open Access Full Text Article

ORIGINAL RESEARCH

Linoleic Acid Reduces Paclitaxel Chemosensitivity in Colorectal Cancer

Bingwen Zhou[1,*], Jinjin Pan[2,*], Mengjie Wang[1,3,*], Peng Zhou[2], Zhili Li[1,4], Jingwei Cui[2], Chuyue Huang[2], Lu Wang[1], Zhimin Fan[1]

[1]Jiangsu Clinical Innovation Center for Anorectal Diseases of TCM, Nanjing Hospital of Chinese Medicine Affiliated to Nanjing University of Chinese Medicine, Nanjing, People's Republic of China; [2]Anorectal Center, Nanjing Hospital of Chinese Medicine affiliated to Nanjing University of Chinese Medicine, Nanjing, People's Republic of China; [3]Anorectum Department, Kunshan Integrated Chinese and Western Medicine Hospital, Kunshan, People's Republic of China; [4]Anorectum Department, Jinan Municipal Hospital of Traditional Chinese Medicine, Jinan, People's Republic of China

*These authors contributed equally to this work

Correspondence: Zhimin Fan; Lu Wang, Email fanzm@njucm.edu.cn; wanglu@njucm.edu.cn

Purpose: Paclitaxel, a natural diterpenoid compound derived from *Taxus* species, is one of the most successful plant-based anticancer drugs and has been widely applied in the treatment of various solid tumors. In recent years, emerging evidence has suggested its potential efficacy in refractory or advanced colorectal cancer (CRC), particularly in patients resistant to standard first-line chemotherapy such as 5-fluorouracil (5-FU). However, responses to paclitaxel in CRC are heterogeneous. This study aimed to elucidate the metabolic determinants underlying the heterogeneous response of CRC to paclitaxel and to identify serum metabolites associated with therapeutic response.

Patients and Methods: Integrated serum metabolomic profiling was performed in patient-derived tumor organoid (PDTOs, n=18), combined with drug sensitivity assays and in vivo validation using mouse xenograft models. An analysis was conducted to sensitivity of paclitaxel, followed by targeted metabolomic quantification and pathway enrichment to identify key metabolites influencing paclitaxel efficacy.

Results: Linoleic acid (LA) was identified as a serum metabolite significantly correlated with reduced paclitaxel sensitivity. Elevated LA levels attenuated paclitaxel-induced G_2/M cell cycle arrest and reduced cytotoxicity by altering microtubule dynamics. Functional validation in CRC cell lines and animal models further confirmed that LA diminished the antitumor effect of paclitaxel, supporting a metabolism-mediated mechanism of chemoresistance.

Conclusion: This study identifies serum linoleic acid as a metabolism-related candidate biomarker associated with paclitaxel resistance in CRC. These findings highlight the potential clinical relevance of metabolic factors in modulating chemotherapy response and suggest that LA may have potential relevance for patient stratification in future studies of paclitaxel response in CRC.

Keywords: chemosensitivity, patient derived tumor organoids, serum metabolomics, personalized treatment, biomarker, colorectal cancer

Introduction

Paclitaxel, a natural anticancer agent derived from Taxus chinensis, has demonstrated significant therapeutic efficacy in various solid tumors, including gastric, liver, lung, and breast cancers.[1–4] Its primary mechanism involves binding to the amino terminus of β-tubulin to stabilize microtubules, thereby disrupting mitosis and inducing apoptosis.[5] Although paclitaxel is not part of the standard first-line chemotherapy for colorectal cancer, it has shown therapeutic potential in patients with refractory or treatment-resistant disease and is often explored in second-line or combination regimens. Owing to its well-characterized mechanism of action, paclitaxel also serves as a prototypical model compound for investigating how metabolic states modulate the efficacy of microtubule-directed chemotherapy.[6–9] Understanding how metabolic states modulate the activity of these agents could therefore provide mechanistic insights and inform novel strategies to overcome drug resistance in colorectal cancer.

https://doi.org/10.2147/DDDT.S577058
Received: 21 November 2025
Accepted: 20 April 2026
Published: 28 April 2026

Colorectal cancer (CRC) ranks as the third most prevalent malignancy globally, with millions of individuals being diagnosed annually.[10] Standard management involves surgical resection combined with adjuvant chemotherapy, while systemic chemotherapy remains central for advanced disease. However, despite well-established treatment guidelines, not all patients derive optimal benefit from standard chemotherapy regimens. Clinical data indicate that mainstream regimens, including FOLFOX, CAPOX, and FOLFIRI, achieve meaningful responses in only approximately one-third of patients, while the remainder experience minimal therapeutic benefit.[11] The core components of these regimens, such as 5-fluorouracil (5-FU) and oxaliplatin, also frequently encounter resistance during treatment, which significantly compromises clinical efficacy.[12,13] These observations highlight the substantial inter-patient heterogeneity in chemotherapy response and underscore an urgent need for predictive biomarkers to guide treatment selection and improve therapeutic outcomes in CRC.

Patient-derived tumor organoids (PDTOs) are three-dimensional in vitro cultures generated from tumor tissues obtained directly from cancer patients. Compared with conventional tumor models, PDTOs better preserve the genetic, histological, and molecular characteristics of the original tumor, including its inherent heterogeneity.[14] As a result, they have become powerful tools in cancer research, translational medicine, and drug development.[15] A major clinical advantage of PDTOs lies in their ability to accurately predict individual responses to chemotherapy, thereby helping to maximize therapeutic efficacy while minimizing treatment-related toxicity.[16–20] In a comparative study, Yao et al analyzed organoid-based drug sensitivity data alongside clinical outcomes in patients with locally advanced CRC who received adjuvant chemotherapy and reported a concordance rate of 84.43% between organoid predictions and actual clinical responses.[21] Similar findings were reported in a landmark study published in Science in 2018, which demonstrated that organoid-based assays could predict drug sensitivity with high sensitivity and specificity.[22] Collectively, these studies establish PDTOs as a reliable preclinical platform for evaluating chemotherapeutic efficacy and support their use in investigating how metabolic factors influence drug response in colorectal cancer.

Accumulating evidence indicates that metabolic reprogramming, particularly lipid metabolism, plays a critical role in cancer progression and therapeutic response.[23,24] Alterations in fatty acid composition can influence membrane properties, cytoskeletal organization, and drug responsiveness in tumor cells. Linoleic acid (LA), a major ω-6 polyunsaturated fatty acid in circulation and membrane phospholipids, has been implicated in cancer-related biological processes and may modulate cellular sensitivity to anticancer therapies.[25,26] Experimental studies have shown that polyunsaturated fatty acids can regulate microtubule dynamics and cytoskeletal plasticity, suggesting a potential interaction between lipid metabolic status and the efficacy of microtubule-targeting agents such as taxanes.[27] However, whether circulating LA levels affect paclitaxel sensitivity in colorectal cancer has not been systematically investigated. In parallel, metabolomics has emerged as a powerful approach for capturing systemic metabolic states and identifying biomarkers predictive of therapeutic response.[28,29] Metabolomic profiling of serum or plasma has been successfully applied to stratify patients according to chemotherapy sensitivity and clinical outcome across multiple cancer types.[30] Integrating metabolomic signatures with functional drug-response assays therefore provides a rational strategy to uncover metabolism-driven determinants of inter-patient heterogeneity in chemotherapeutic response.

In our previous clinical observations, we found that some colorectal cancer patients who were resistant to 5-FU exhibited notable sensitivity to paclitaxel. Building on these findings, we designed the present study to systematically investigate the metabolic determinants of paclitaxel response. We collected tumor tissues and matched serum samples from these patients to establish patient-derived tumor organoids (PDTOs) and performed comprehensive serum metabolomic profiling. This study was designed to identify metabolic biomarkers predictive of paclitaxel sensitivity and to elucidate the metabolic determinants of its efficacy in colorectal cancer. Linking metabolomic signatures with functional organoid-based responses provides mechanistic insight into metabolism-mediated variability in drug response and establishes a foundation for expanding the therapeutic use of paclitaxel in colorectal cancer management.

Materials and Methods

Samples and Patients

The tumor specimens were obtained from patients with CRC who underwent surgical resection at Nanjing Hospital of Chinese Medicine affiliated to Nanjing University of Chinese Medicine. Prior to sample collection, all patients provided written

informed consent for the utilization of clinical data and surgical samples in accordance with the principles outlined in the Declaration of Helsinki. Following surgical resection of the tumor, the majority of patients underwent administration of standard chemotherapy regimens. The surgically resected samples were divided into three sections. One portion was stored in cryotubes at −80°C for whole-exome sequencing analysis (WES). Another piece was fixed in 4% paraformaldehyde for histopathological and immunohistochemical staining. The final section was immersed in a solution containing 10 nM HEPES (Gibco, 15630130), 100 U/mL penicillin streptomycin-amphotericin B (Beyotime, C0224), and 10 μM Y-27632 (MedChemExpress, HY-10071, USA), and was utilized for organoid generation. Simultaneously, 3mL of blood samples were collected for the purpose of conducting metabonomics research. Serum samples were collected under standardized pre-analytical conditions. All participants underwent overnight fasting prior to blood collection, and samples were obtained in the morning using uniform procedures to minimize dietary and circadian variability. This study adhered to the national guidelines and received approval from the Nanjing Hospital of Chinese Medicine affiliated to Nanjing University of Chinese Medicine Ethics Committee (Approval No.: KY2022309).

Organoid Culture

Tumor tissues were rinsed with PBS, then treated repeatedly with penicillin-streptomycin-amphotericin B DMEM/F12 (Gibco, USA) medium until clean. The petri dish was pre-cooled, and the cleaning solution was discarded post-use. The tissue was transferred into the pre-cooled petri dish with sufficient medium to preserve moisture during mincing. A sterile scalpel was used to mince the tissue into small pieces, which were then transferred to a petri dish with 3mL digestion solution. The tissue pieces were agitated with a pipettor gun before being transferred to a 15mL centrifuge tube. Shaking at room temperature for 10–15 minutes dissociated the tissue into single cells or small cell clusters. The cell suspension was then placed on ice, 3mL of DMEM/F12 was added to stop the digestion, and after incubation, the tissue was separated from the cell suspension by gentle pipetting. The supernatant was then centrifuged for separation. Before centrifugation, the centrifuge was pre-cooled to 4 °C to preserve sample integrity. Centrifugation was performed at 1400 rpm for 5 minutes to separate aggregated tumor cell clusters. The old medium was discarded, then the supernatant was added, and 3 mL of medium per tube was transferred to the previous medium, restarting the centrifugation process. This procedure was repeated twice more for a total of three centrifugation cycles to reduce residual digestion. After the supernatant was completely removed, the tumor cells were combined with the matrix adhesive in a 1:2 volume ratio, taking care to avoid air bubble entrapment. The resulting suspension was seeded into 6-well culture plates and incubated for 15 minutes. Following incubation, 2 mL of culture medium was added to each well, and the cells were cultured with medium exchange every two days. All experiments were performed with mycoplasma-free cells.

Histology and Immunostaining

Four percent of fresh paraformaldehyde-fixed tumor tissue, subjected to 24-hour dehydration, was embedded in paraffin blocks. Subsequently, after medium removal, the organoids were immobilized in 4% newly prepared paraformaldehyde for a duration of 12 hours. A 3% agarose solution was prepared in TBST and was heated to the boiling point using a microwave oven. Following a designated incubation period within an agarose matrix, the tissue specimen was allowed to cool, subsequent to which it was immobilized via paraffin embedding. This process was preceded by dehydration and followed by paraffin sectioning, culminating in the application of hematoxylin and eosin (H&E) staining for histological characterization. Immunohistochemical staining (IHC) was performed using specific antibodies against Ki67, CK20, and SMA. Appropriate baking sheets were used for dewaxing, and a rigorous dehydration process was conducted to maintain tissue integrity. Sodium citrate buffer was heated to boiling, simmered for 20 minutes, and then cooled naturally to room temperature. Cells were washed three times with PBS for 5 minutes each, after which 3% hydrogen peroxide was added dropwise, and samples were incubated for 20 minutes at room temperature. Another triple PBS wash was performed, and pre-diluted primary antibodies were added to incubate overnight at 4°C in a wet box. Cells were washed with PBS to remove unbound antibodies and were then incubated for 60 minutes at room temperature. DAB chromogenic developer was added after three more PBS washes, color development was observed under a microscope, and the samples were rinsed with distilled water when the reaction was complete. Dehydration, clearing, and mounting were subsequently performed after the blue-red color fades.

WES Analysis

Whole exome sequencing was conducted utilizing the BGISEQ-500 sequencing platform. Qualified genomic DNA samples were randomly fragmented with an ultrasonic high-performance sample preparation system. DNA fragments of approximately 150bp-250bp in length were selected for terminal repair, followed by the addition of an "A" base at the 3′ end. Subsequently, both ends of the fragments were ligated with library adapters to prepare a linear amplification-based A-tailed library. A Qubit 2.0 fluorometer and the ssDNA detection kit were employed to assess the concentration of the DNA library, and successful library construction was confirmed when concentrations exceeded 0.64 ng/uL. An optimal quantity of the hybridization library and the exon array were selectively captured and enriched, after which the under-enriched fragments were washed and amplified. Following stringent quality control, an adequate number of amplification products were selected and arranged sequentially to ensure the integrity of the dataset.

Drug Response Assay

High-quality organoid cultures, characterized by robust growth indices, were meticulously selected to guarantee a sufficient quantity and functional integrity for subsequent experiments. The cell culture medium was processed and enzymatically digested with trypsin to isolate single cells. Cell suspensions containing 5% Matrigel (Corning, USA) were seeded at a density of 1000 cells per well in 384-well plates. After an incubation period of 24h at 37°C with 5% CO2, 384-well plates were utilized to culture the organ classes, followed by a 48h exposure to the test drugs in the presence of DMSO as a control. The concentration gradient of paclitaxel (Qilu, China) and 5-FU (Jinyao, China) spanned from 10nmol/L to 10000nmol/L, with five distinct concentration points. The upper micromolar range was included because drug penetration in 3D organoids embedded in Matrigel is limited, often requiring higher testing concentrations than 2D cultures.[31] Upon completion of drug administration, cellular viability was assessed utilizing the CellTiter-Glo 3D luminescent cell viability assay kit, and the resulting data were normalized and expressed as percentage cell viability. Dose-response curves were fitted in GraphPad Prism version 8.0 using a four-parameter logistic model with variable slope on log10-transformed drug concentrations. For each PDO, three technical replicate wells were measured at each concentration and entered into GraphPad Prism as replicate response values at the corresponding concentration. Curve fitting and IC50 estimation were performed independently for each PDO, which was treated as a biological replicate. Default fitting settings were used, with no additional weighting applied. Drug-response assays were performed on all 24 patient-derived colorectal cancer organoid lines. For downstream statistical analyses, each organoid line was treated as a single biological replicate. The primary outcome of this study was drug response, quantified as the log10-transformed IC50 value derived from dose-response curves of patient-derived tumor organoids. In some PDOs, the estimated IC50 exceeded the maximum tested concentration range, indicating that the true IC50 was beyond the experimental dynamic range. These cases were considered right-censored (>maximum tested concentration). For primary IC50-based analyses, only PDOs with estimable IC50 values were included. As a prespecified sensitivity analysis, the area under the dose-response curve (AUC) was calculated for each PDO using the trapezoidal rule over log 10-transformed concentrations. AUC is used as an alternative response indicator for targeted metabolomics assessment, and is employed to confirm the reliability of the correlation between serum linoleic acid and paclitaxel in the IC50 assessment.

Blood Samples

200μL serum were combined with 400μL pre-cooled methanol (−20°C), subjected to vortex mixing for 1min, and then centrifuged at 12000rpm/min for 10min at 4°C. Subsequently, the entire supernatant was aspirated and transferred to a new centrifuge tube. Following concentration and evaporation of the supernatant, 160μL of a 2-chloro-L-phenylalanine solution, prepared in a mixture of 80% methanol, was subsequently added. After sample dissolution, the supernatant exceeding 0.22 micrometers was filtered through a nylon syringe filter, and the resulting filtrate was analyzed by UPLC-QTOF-MS/MS to collect metabolite information. Pooled quality control (QC) serum samples were prepared by mixing equal aliquots from all study samples and were injected periodically throughout the analytical run. QC samples were used to assess instrument stability and correct signal drift.

Metabolomics Method

An ultra-high performance liquid chromatograph (Thermo Vanquish) equipped with a T3 chromatographic column (Waters, 2.1×150mm, 1.8μm) was utilized, maintaining a flow rate of 0.25mL/min and a column temperature of 40°C, with a sample volume of 2μL. In positive ion mode, the mobile phase was 0.1% formic acid acetonitrile (C) and 0.1% formic acid water (D), and the gradient elution program was as follows: 0–1 min, 2% C; 1–9 min, 2% - 50% C; 9–12 min, 50% - 98% C; 12–13.5 min, 98% C; 13.5–14 min, 98% - 2% C; 14–20 min at 2% C. Negative ion mode, the mobile phase of acetonitrile (A) and 5mM ammonium formate water (B), gradient elution procedure was: 0–1min, 2% A; 1–9min, 2% - 50% A; 9–12min, 50% - 98% A; 12–13.5 min, 98% A; 13.5–14 min, 98% - 2% A; 14–17min, 2% A.

An electrospray ion source (ESI) was coupled with the mass spectrometer detector (Thermo Orbitrap Exploris 120), data acquisition was performed in both positive and negative ion modes. The positive ion spray voltage was 3.50 kV, the negative ion spray voltage was −2.50 kV, the sheath gas was 30 arb, and the auxiliary gas was 10 arb. The capillary temperature was set at 325°C. The first stage employed full scanning with a resolution of 60000 and the ion scanning range was from 100 to 1000. For the second stage, lysis was conducted using HCD with a collision voltage set at 30%. The resolution for the second stage was 15000 and signal acquisition involved breaking four ions. Additionally, dynamic exclusion was utilized to remove unnecessary MS/MS ions.

Targeted Quantitative Validation of Candidate Metabolites

Targeted metabolite quantification was performed on an Agilent 7890A/5975C GC–MS system. Samples were separated on a DB-5MS capillary column (30 m × 0.25 mm ID × 0.25 μm). The carrier gas was high-purity helium at a constant flow of 1.0 mL/min. The inlet temperature was 250 °C, and injections were made in splitless mode. The oven program started at 40 °C (held 1 min), increased at 7 °C/min to 300 °C, and was then held for 2 min. A 10-min solvent delay was applied.

Mass spectrometric detection was carried out with electron-impact (EI) ionization at 70 eV. The ion source, transfer line, and quadrupole temperatures were set to 230 °C, 300 °C, and 150 °C, respectively. Data acquisition was performed in selected-ion monitoring (SIM) mode, monitoring m/z 75 and 257 for quantification/confirmation. Peaks were integrated and exported for downstream quantitative analysis under these fixed acquisition conditions.

Data Analysis

Original mass spectrometry data were processed using the MSConvert tool from the Proteowizard package (version 3.0.8789) to facilitate the conversion into an offload file, suitable for the mzXML file format. RXCMS (version 3.7.1) software was used for peak detection, peak filtering, and peak alignment to obtain the quantitative list of substances. The parameters were set as bw=2, ppm=15, peakwidth=c(5,30), mzwid=0.015, mzdiff=0.01, method= “centWave”, and all other parameters use default values. The public databases HMDB, massbank, LipidMaps, mzcloud, KEGG and self-built material database were used to identify the substances, and the parameter was set as ppm < 30 ppm. A LOESS-based signal correction approach was applied using QC injection order to adjust for systematic intensity variation. Metabolic features with a RSD greater than 30% in QC samples were excluded from further analysis. Prior to statistical analysis, metabolite intensities were normalized using an internal standard and log-transformed to reduce skewness and approximate normality. All statistical analyses of metabolomics data were performed on log-transformed values. Paclitaxel response was treated as a continuous variable, associations between serum metabolite abundance and paclitaxel response were primarily assessed using Spearman correlation analysis with false discovery rate (FDR) control. Metabolites were prioritized based on the magnitude and direction of correlation coefficients, while FDR-adjusted p-values were reported to account for multiple testing. For sensitivity assessment, samples were additionally stratified using median and quartile cutoffs of IC50 values. These stratified analyses were used to evaluate the consistency and robustness of associations identified in the primary correlation analysis, rather than as independent selection criteria. The metabolites subjected to targeted validation were also analyzed using Spearman correlation analysis, and a leave-one-out sensitivity analysis was performed for to evaluate the influence of individual samples. Correlation coefficients were recalculated after sequential exclusion of each observation. No statistical outliers were removed beyond predefined exclusions related to experimental quality control.

Pathway Enrichment

The MetaboAnalyst package was used to perform pathway enrichment and topology analysis. Utilizing the KEGG Mapper visualization tools, the MetPA database facilitated the exploration of metabolic pathways and circuit diagrams. Through comprehensive pathway enrichment and topological analyses, it identified potential metabolic pathways altered by biological perturbations. Subsequently, the database analyzed the metabolic pathways of interest. Drawing on the outcomes of MetPA assessments, relative response values of the metabolic pathways were derived by comparing the relative response values of the identified metabolites and employing a dimensionality reduction algorithm. Additionally, correlation coefficients among metabolic pathways were computed, enabling the delineation of a metabolic pathway association network.

The Effect of Linoleic Acid on Paclitaxel Chemosensitivity

All cells were cultured in RPMI-1640 (Gibco, USA) medium supplemented with 10% fetal bovine serum and maintained at 37°C in an atmosphere of 5% CO2. The experiment consisted of three groups, each with three parallel replicates: the control group (DMSO treatment), the Paclitaxel group (22 nM), and the Paclitaxel and LA (Yuanye, China) combination treatment group (LA concentration range of 10–1000 nM). In the combination treatment group, cells were initially treated with LA for 24 hours, followed by the addition of Paclitaxel. After 48 hours of treatment, cell viability was assessed using the Cell Counting Kit-8 (CCK-8) assay, and cell survival rates were calculated by determining the optical density (OD) at 570 nm. Cell viability experiments were performed with six independent biological replicates, consistent with standard practice for quantitative cell-based assays to ensure adequate statistical reliability. Each independent experiment was considered a biological replicate. Technical replicates within each experiment were averaged prior to statistical analysis.

Effects of Linoleic Acid and Paclitaxel on Microtubule Structure

All cells were seeded on coverslips or in cell culture plates for microtubule structure observation. The experimental groups were identical to those used in the cell viability assay and included the control group (DMSO treatment), the Paclitaxel group (22 nM), the LA group (1000 nM), and the combination treatment group. After 24 hours of drug treatment, cells were fixed with 4% paraformaldehyde and then permeabilized with 0.1% Triton X-100. The cells were then incubated with a primary antibody against α-tubulin (AB7291, Abcam Plc), followed by detection using a fluorescence-conjugated secondary antibody, and the cell nuclei were stained with DAPI. Fluorescence or confocal microscopy was employed to observe and record the microtubule morphology in each group, focusing on analyzing the stability and structural changes of microtubules in the Paclitaxel and combination treatment groups. Three independent experiments were performed for exploratory analyses. Measurements obtained from technical replicates with each experiment were averaged before statistical analysis.

Effects of Linoleic Acid and Paclitaxel on the Cell Cycle

All cells were seeded into 6-well plates and treated according to the experimental groups established in the cell viability assay. After 24 hours of incubation, the cells were collected. Following PBS washing, cells were fixed with 70% cold ethanol and incubated at 4°C for 1 hour. After fixation, cells were washed once more with PBS and stained with a solution containing propidium iodide (PI) and RNase to degrade RNA, followed by incubation in the dark for 30 minutes. Cell DNA content and cell cycle distribution were analyzed by flow cytometry with excitation at 488 nm to detect red fluorescence. The cell cycle was assessed using the PI single staining method, and the Cell Cycle Detection Kit (KGA511, KeyGEN BioTECH) was employed. Three independent experiments were performed for exploratory analyses. Measurements obtained from technical replicates with each experiment were averaged before statistical analysis.

Animal Experiments

Female BALB/c mice (6–8 weeks old) were used to establish a subcutaneous tumor model. CT26 cells were suspended in PBS at a concentration of 5×10^7 cells/mL, and 1×10^6 cells in 100 μL were injected subcutaneously into the right forelimb of each mouse. When tumors reached approximately 100 mm^3, mice were randomly allocated into four groups

(n = 6 per group) using a simple randomization method: control, paclitaxel (10 mg/kg), linoleic acid (100 mg/kg), and the combination treatment (paclitaxel 10 mg/kg + linoleic acid 100 mg/kg). The sample size (n = 6 per group) was determined based on prior experience with xenograft models and expected effect sizes observed in similar preclinical studies, while adhering to ethical principles to minimize animal use. Linoleic acid was administered daily by oral gavage at 100 mg/kg dissolved in medium-chain triglyceride oil, starting from day 0. Paclitaxel was administered intraperitoneally at 10 mg/kg once weekly on days 7, 14, and 21. On the days of chemotherapy, linoleic acid was given first, followed 3 hours later by paclitaxel injection. Control and paclitaxel groups received equal volumes of medium-chain triglyceride oil by gavage, whereas the linoleic acid group received only linoleic acid by gavage. All mice were maintained on a standardized low-linoleic acid diet. Tumor length and width were measured with calipers every two days beginning one week after inoculation, and tumor volume was calculated as $V = (\text{length} \times \text{width}^2)/2$. The experimental endpoint was defined as day 21, when the largest tumor volume reached approximately 2000 mm^3. After the final administration of paclitaxel on day 21, the mice were anesthetized with isoflurane and then humanely euthanized by cervical dislocation, after which blood samples were collected and tumors were excised for subsequent analyses. Blinding was not applied during treatment administration. Tumor volume measurements and image quantification were performed without blinding to treatment allocation. All animal procedures were conducted in accordance with the Guidelines for the Ethical Review of Laboratory Animal Welfare (China, 2018) and the AVMA Guidelines for the Euthanasia of Animals, and were approved by the Animal Ethics Committee of Nanjing University of Chinese Medicine (protocol code ACU211202). Each mouse was considered an independent experiment unit for statistical analysis.

Data Statistics

For cell-based and in vivo experiments, continuous outcomes are presented as means ± standard deviations (SD) unless otherwise specified. All statistical analyses were conducted using GraphPad Prism software (version 8.0) and R (Version 4.4.1) for bootstrap resampling procedures. For experiments with five or more independent biological replicates, statistical analyses were performed according to the experimental design. Factorial designs were analyzed using two-way ANOVA with paclitaxel treatment and linoleic acid as fixed factors, and interaction effects were tested. Linoleic acid dose–response experiments under paclitaxel treatment were analyzed using one-way ANOVA followed by Dunnett's multiple-comparison test with the paclitaxel-only group as the reference. Where applicable, unpaired Student's t-tests were used for prespecified comparisons. Normality was assessed using the Shapiro–Wilk test. In small sample settings, this was complemented by visual inspection of Q–Q plots, given the limited power of formal normality tests. When model assumptions were not satisfied, prespecified alternative approaches were applied. For unequal variances, Welch's *t*-test or Welch's ANOVA was used as appropriate. In cases of clear non-normality or influential outliers in small sample settings, data transformation or nonparametric methods were considered. Where applicable, diagnostic assessments were performed at the level of model residuals. Experiments with fewer than five independent biological replicates, including microtubule morphology and cell-cycle distribution analyses, are presented as exploratory analyses. In these cases, uncertainty was estimated using nonparametric bootstrap confidence intervals based on 10,000 resamples with a two-sided percentile method. Effect sizes and corresponding 95% bootstrap confidence intervals are reported without reliance on parametric hypothesis testing. To control for multiplicity, hypothesis families were defined by experimental endpoint and figure. The primary prespecified contrast was the comparison between paclitaxel alone and paclitaxel combined with linoleic acid within each experimental system. Other pairwise comparisons were considered supportive and interpreted within the context of the overall model. Longitudinal tumour volume data were analysed using a linear mixed-effects model fitted with the lme4 and lmerTest packages in R. Tumour volume was analysed on the original scale. Time (day) was treated as a continuous variable. Treatment group, day, and their interaction were included as fixed effects, with mouse identity as a random intercept. Type III ANOVA with Satterthwaite approximation was used for inference. Post hoc comparisons of group-specific slopes were conducted using estimated marginal trends with Tukey adjustment. Model assumptions were assessed using residual diagnostics. Endpoint tumour volume and tumour weight were analysed as secondary outcomes using two-way ANOVA with prespecified post hoc testing. For all inferential analyses, the independent unit of analysis was the biological replicate.

Results

Patient Samples and Clinical Data

The tumor samples used in this study were collected from November 2021 to November 2023 at the Anorectal center of Nanjing Hospital of Chinese Medicine affiliated to Nanjing University of Chinese Medicine, focusing on CRC patients admitted to the hospital. 24 patient-derived CRC organoids were successfully generated, demonstrating robust growth and consistent passage maintenance. The gender distribution among the 24 patients was equally divided, with 12 females and 12 males. The age of the participants spanned from 37 to 89 years, with an average age of 66 years. The cohort consisted of 10 cases of rectal cancer and 14 cases of colon cancer. The mean body mass index (BMI) was 23.9. The patient dataset comprised 4 cases at pathological stage I, 11 at stage II, 8 at stage III and a sole case at stage IV. All 24 biopsy samples were histopathologically confirmed as adenocarcinoma, which included a rare instance of rectal protuberant mucinous adenocarcinoma. Tumor pathology was identified by the Department of Pathology of Nanjing Hospital of Chinese Medicine affiliated to Nanjing University of Chinese Medicine. Clinical information is provided in Table 1. The subsequent handling, exclusions, and allocation of all samples and organoids are summarized in Table 2.

Establishment and Histological Characterization of CRC PDTOs

To assess the sensitivity of clinical chemotherapy drugs, we established a patient-derived tumor organoid (PDTO) model using colorectal cancer tissues from 24 patients. The organoids were observed under an optical microscope throughout the culture process, and all 24 samples exhibited robust growth. The more stable organoid cell morphologies predominantly included thin-walled cystic structures, thick-walled cystic structures, and dense spherical structures, with a minor portion appearing vacuolar. As the organoids grew, the volume of the vacuolar structures gradually increased, while the density of the cystic and spherical structures showed a significant increase (Figure 1A). Notably, there were substantial morphological differences between the first and second generations of some organoids, with the second generation exhibiting more vacuolar shapes that were relatively uniform and increased significantly in volume as they grew (Figure 1B). Two well-growing tumor organoids and their corresponding tumor tissues were selected for paraffin-embedded section staining. Comparison of hematoxylin and eosin (HE)-stained sections revealed that patient-derived colorectal cancer organoids retained the morphological characteristics of the original tumor tissues, with the nuclei and overall cell morphology closely matching those of the source tissues (Figure 1C). We performed immunohistochemical staining using two common tumor markers, Ki67 and CK20, along with a negative control marker, SMA. Ki67 is a nuclear protein present only in dividing cells and serves as a marker for cell proliferation, with higher values indicating faster tumor growth and higher malignancy. CK20, or cytokeratin 20, is an epithelial-specific marker frequently used for

Table 1 Baseline Patient and Tumor Characteristics

Characteristic	N=24 Patients
Age, Median (range), years	66(37–89)
Sex, No (%)	
Male	12(50)
Female	12(50)
BMI, median (range), kg/m^2	23.9(18.31–30.86)
Tumor site, No (%)	
Colon	14(58.3)
Rectum	10(41.7)
Pathological Stage No (%)	
I	4(16.7)
II	11(45.8)
III	8(33.3)
IV	1(4.2)
Pathological type	
Adenocarcinoma	24

Table 2 Flow of Patient-Derived Organoids and Serum Samples

Step	Number	Notes
CRC patients enrolled	24	Surgical samples collected
PDOs	24	Used for drug screening
Excluded from IC50-based analyses	6	IC50 not determinable or missing matched serum
Final PDO-serum pairs	18	Used for metabolomics analyses
Discovery cohort (untargeted metabolomics)	10	Randomly selected
Validation cohort (targeted quantification)	8	Independent samples

colorectal cancer. SMA, a myogenic marker, served as a negative control and was not expressed in colorectal cancer organoids. The results shown in Figure 1C indicated positive expression of Ki67 and CK20 in both tumor tissues and organoids, while SMA expression was negative. These findings confirmed the accuracy of the colorectal cancer organoids as being derived from the original tumor tissues through the identification of histological characteristics associated with colorectal cancer tumor marker expression.

Genomic Characterization of CRC PDTOs

Previous studies have indicated that organoids derived from cancer patients replicate the genomic characteristics of the corresponding tumor tissues.[32] In this study, we selected two colorectal cancer organoids and their corresponding tumor tissues for whole-exome sequencing. The sequence comparison results for the four samples showed a mapping ratio of over 99.9% to the reference genome, reflecting high-quality sequencing data. Analysis of mutations (SNV + InDel) revealed that the mutation proportions between each organoid and its corresponding tissue were highly consistent (Figure 2A and B). InDel detection showed that the length and proportion of insertion and deletion mutations in tumor tissues and organoids were remarkably similar (Figure 2C and D). Additionally, CNV analysis demonstrated a high degree of similarity in copy number variations between tumor tissues and their derived organoids, with significant differences observed between different groups (Figure 2E). These findings confirm that the constructed colorectal cancer organoids preserve the genomic characteristics of the original tumor tissues.

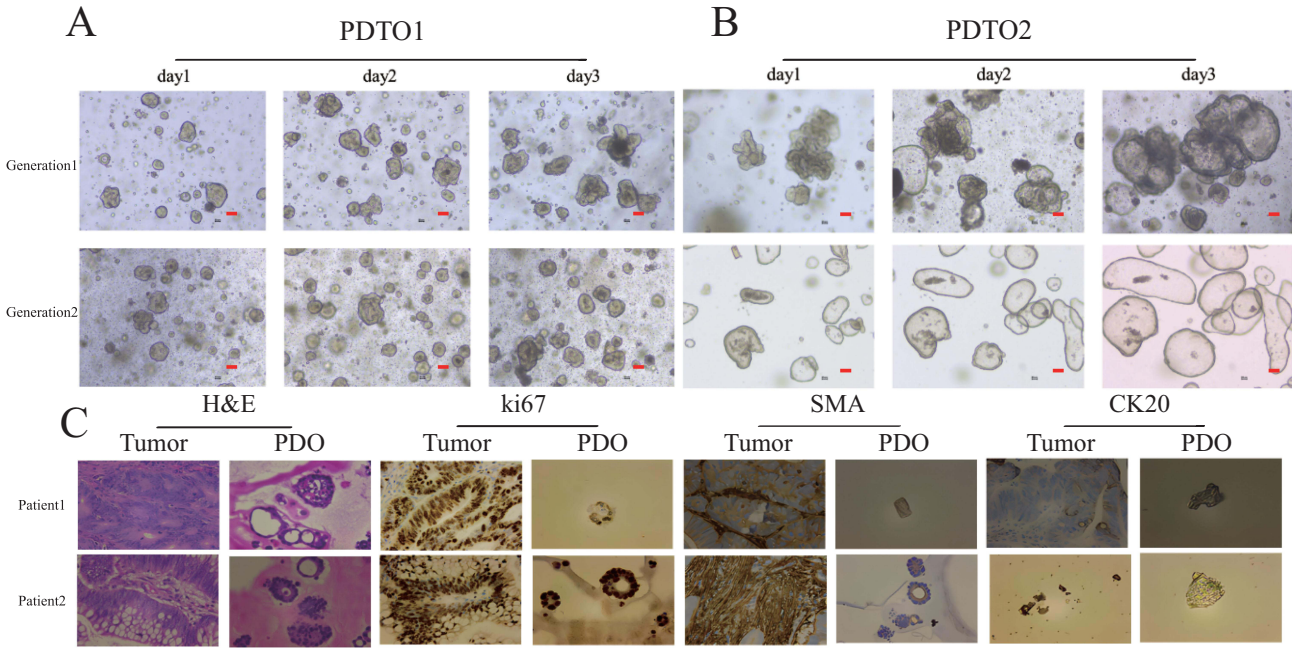

Figure 1 Establishment of organoids and immunohistochemical characterization. (**A** and **B**) Morphological changes of two primary organoids and their passage organoids captured by high-content imaging, with red markings representing 100 μm. (**C**) Immunohistochemical staining of two organoids and their corresponding tumors.

https://doi.org/10.2147/DDDT.S577058

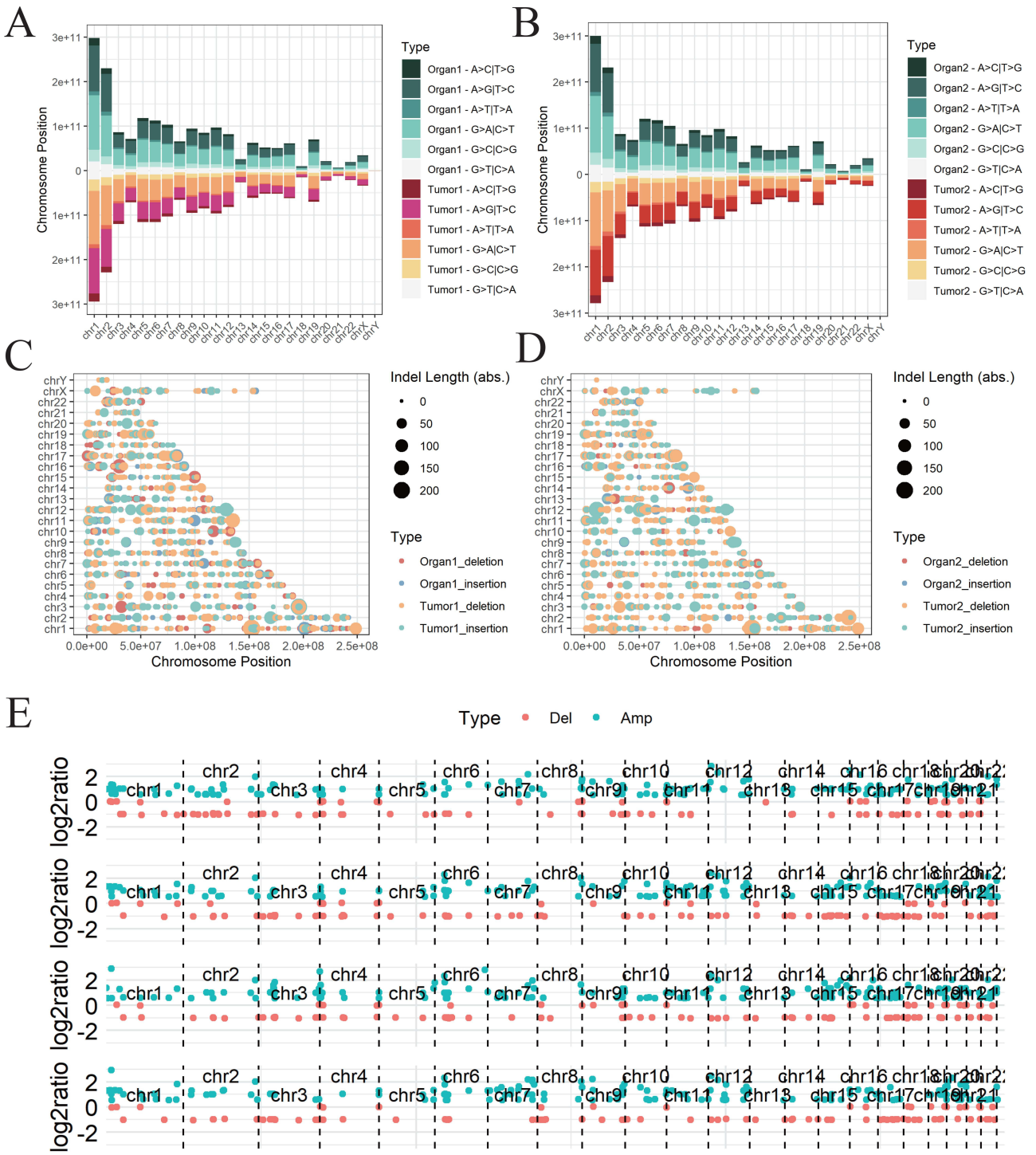

Figure 2 Genetic profiles of organoids and tumor tissues. (**A** and **B**) SNP mutation profiles of two organoids and their corresponding tumor tissues. Green indicates gene mutations in organoids, while red indicates gene mutations in tumors. (**C** and **D**) InDel mutation profiles of two organoids and their corresponding tissues. Red indicates gene deletions in organoids, blue indicates gene insertions in organoids, Orange represents gene deletions in tumor tissues, and green represents gene insertions in tumor tissues. (**E**) CNV profiles of two organoids and their corresponding tissues. Red indicates gene deletions, and green indicates gene amplifications.

Drug Screening in CRC PDOs

In this study, drug sensitivity tests were conducted on 24 patient-derived tumor organoids (PDTOs) using Paclitaxel and 5-FU. High-content imaging technology was employed to capture detailed images of the organoids before and after drug treatment. The results indicated that the majority of organoids exhibited higher sensitivity to Paclitaxel compared to

https://doi.org/10.2147/DDDT.S577058

5-FU. Among those sensitive to Paclitaxel, a bimodal distribution of sensitivity was observed, suggesting varied responses among the organoids. Two representative organoids were selected for detailed analysis. Figure 3A illustrates that, in comparison to the control group, the organoids treated with 5-FU showed no significant changes in volume and density, regardless of the duration of treatment. However, organoids in the Paclitaxel treatment group demonstrated extensive darkening of cells, with blurred boundaries and irregular shapes, indicating a pronounced effect of the drug. The results in Figure 3B demonstrate that, compared to the control group, organoids in the treatment groups exhibited varying degrees of cell death as culture time increased. This was evidenced by darkened cells, irregular edges, and morphological changes resembling ground-glass opacity. The organoids in the Paclitaxel group, in particular, showed extensive cell death and more pronounced growth inhibition than those in the 5-FU group. Additionally, these organoids demonstrated greater sensitivity to Paclitaxel compared to the previously examined organoids. Finally, the half-maximal inhibitory concentration (IC50) values of all organoids were calculated and visualized, as presented in Figure 3C. To evaluate whether common clinical characteristics influenced paclitaxel sensitivity, subgroup analyses were performed according to BMI, age, sex, and tumor stage. As shown in Supplementary Figure S1, none of these variables were significantly associated with changes in paclitaxel IC50, and no significant effect modification was observed across the examined subgroups (BMI, p=0.446; age, p=0.602; sex, p=0.278; stage, p=0.605). These results suggest that paclitaxel sensitivity in PDOs was not driven by these baseline clinical factors. To further assess potential confounding of the linoleic acid–IC50 association, sensitivity linear regression models were fitted with log10(IC50) as the dependent variable and linoleic acid as the independent variable, adjusting for one clinical covariate at a time. The association between linoleic acid and log10(IC50) remained directionally consistent with minimal change in effect size across models (Supplementary Table S1).

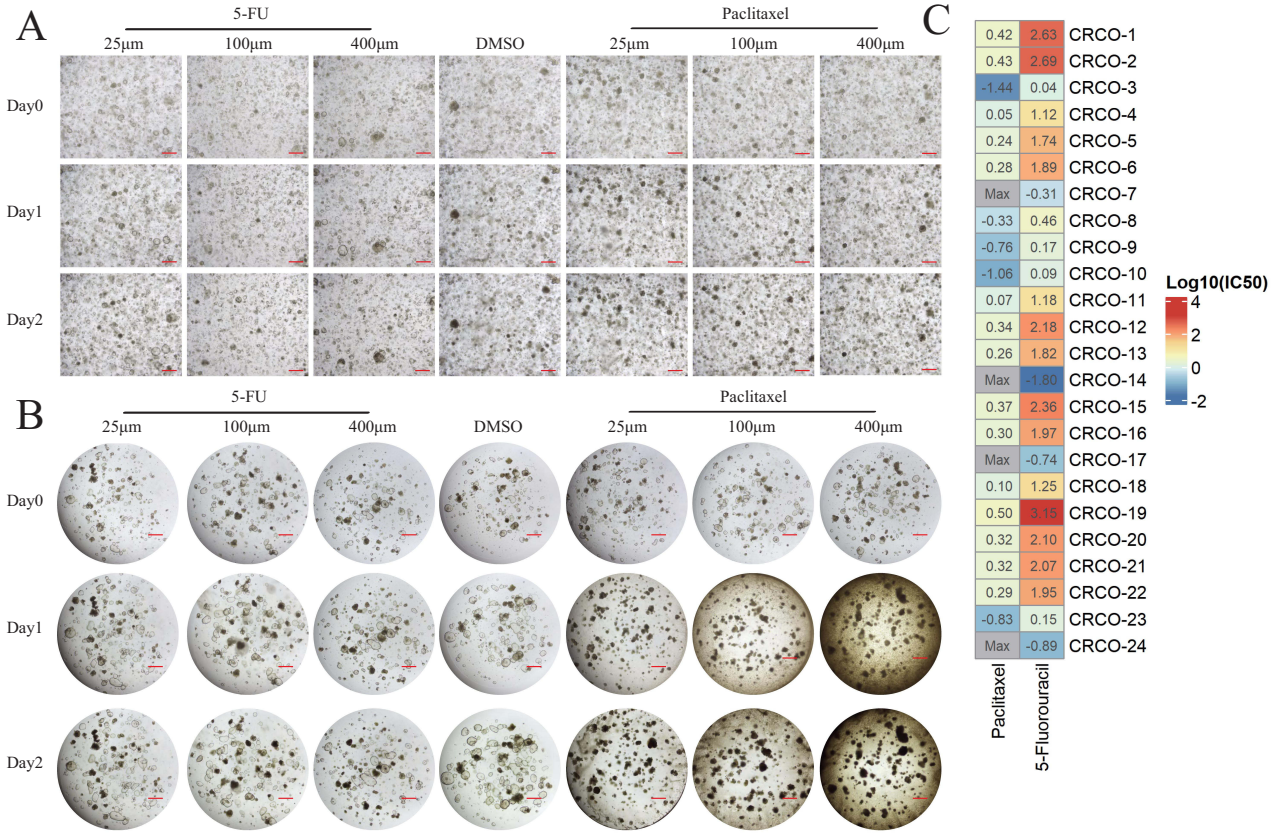

Figure 3 Drug sensitivity assays for Paclitaxel and 5-fluorouracil. (**A** and **B**) Morphological changes in two organoids following treatment with Paclitaxel and 5-fluorouracil, with red markings representing 100 μm. (**C**) Heatmap of Log10-transformed IC50 values for 24 organoids treated with Paclitaxel and 5-fluorouracil. Max indicates IC50 values exceeding the maximum tested concentration range and therefore considered right-censored (>maximum dose). (n=24).

https://doi.org/10.2147/DDDT.S577058

Metabolomics Studies

From the original set of 24 organoids, PDOs in which the paclitaxel IC50 exceeded the maximum tested concentration range were considered right-censored (>maximum dose). For metabolomics analyses, only organoids with estimable IC50 values and available corresponding serum specimens were included, resulting in a total of 18 organoids. From these remaining samples, 10 organoids and their corresponding serum samples were randomly selected as the discovery cohort for untargeted metabolomics analysis. The remaining 8 organoids were subsequently used as the validation cohort for targeted quantification. Paclitaxel response exhibited substantial heterogeneity across organoids and was treated as a continuous variable, quantified by the log10-transformed IC50 values. To identify metabolic features associated with paclitaxel response, associations between serum metabolite abundance and paclitaxel IC50 values were assessed using correlation analysis. Figure 4A summarizes the top 30 metabolites showing the strongest associations with paclitaxel response, with point size representing statistical significance and color indicating the direction and magnitude of correlation. To further visualize inter-organoid drug response heterogeneity, a scatter plot was constructed using the log10-transformed IC50 values of paclitaxel and 5-FU (Figure 4B). For exploratory visualization of metabolic differences across response levels, organoids were additionally categorized into relatively paclitaxel-sensitive and less sensitive groups using the median paclitaxel IC50 value as the cutoff. Untargeted metabolomics analysis was performed on the corresponding serum samples, and the resulting volcano plot is shown in Figure 4C. Based on metabolites associated with paclitaxel response, KEGG pathway enrichment analysis indicated that linoleic acid metabolism and butanoate metabolism were among the pathways potentially involved in paclitaxel sensitivity (Figure 4D). To prioritize robust candidate metabolites, continuous association analysis using Spearman correlation was defined as the primary screening strategy, while stratified analyses based on median and quartile cutoffs were performed as sensitivity analyses. The results of correlation and stratified analyses are summarized in Supplementary Table S2. Candidate metabolites were primarily identified based on continuous Spearman correlation analysis. Figure 4E is presented to illustrate the robustness of these candidates across alternative stratified analyses, rather than as an independent selection criterion. Linoleic acid, oxoglutaric acid, and lithocholic acid showed consistent directionality across stratified analyses. These metabolites were therefore taken forward for targeted quantitative validation, with the stratified analyses providing supportive evidence for robustness. Figure 4F–H illustrate the correlations between these three compounds and paclitaxel sensitivity in the validation cohort. Interestingly, in the validation cohort, the correlations of lithocholic acid and oxoglutaric acid with paclitaxel IC50 values contradicted the trends observed in the discovery cohort, whereas linoleic acid consistently showed a positive correlation (correlation coefficient = 0.752), consistent with the discovery cohort. Leave-one-out sensitivity analysis demonstrated that the direction of the association between linoleic acid and log10(IC50) remained consistently positive after sequential exclusion of each individual sample. The correlation coefficient ranged from 0.40 to 0.86 across iterations, indicating that the observed association was not driven by a single observation (Supplementary Table S3). Taken together, these results suggest that linoleic acid is associated with paclitaxel sensitivity and may serve as a candidate biomarker for further investigation. Sensitivity analysis using AUC as an alternative response metric showed a consistent direction of association for linoleic acid (Figure S2).

Validation of the Impact of Linoleic Acid on Paclitaxel Chemotherapy Sensitivity

To further examine how Paclitaxel and LA affect colorectal cancer cell survival, we treated HCT116, SW480, and SW620 cells with vehicle (control), Paclitaxel, or Paclitaxel combined with increasing concentrations of LA (Figure 5A). The statistical results are recorded in Table S4. Paclitaxel alone significantly decreased cell viability in all three cell lines (all $p < 0.0001$, Dunnett-adjusted). Addition of LA dose-dependently attenuated this effect, with significant rescue observed at higher concentrations (eg., 100nM and 1000nM; $p<0.01$ or $p<0.0001$ depending on the cell line). At 100nM, LA nearly reversed the Paclitaxel-induced reduction in viability. The same pattern appeared in all three lines, indicating that LA effectively counteracts Paclitaxel cytotoxicity. Immunofluorescence staining (Figure 5B) revealed a uniform spindle-like microtubule network in control cells. Paclitaxel triggered pronounced microtubule bundling and intracellular reorganization, giving rise to a compact cell morphology. LA alone produced a relatively loose network without obvious bundles. In the combination group, bundling exceeded that of controls but remained far lower than with Paclitaxel alone, suggesting that LA partially offsets Paclitaxel-mediated microtubule stabilization. Quantification of tubulin fluorescence intensity, branch number, and total microtubule length (Figure 5C–E) indicated that Paclitaxel increased all three metrics

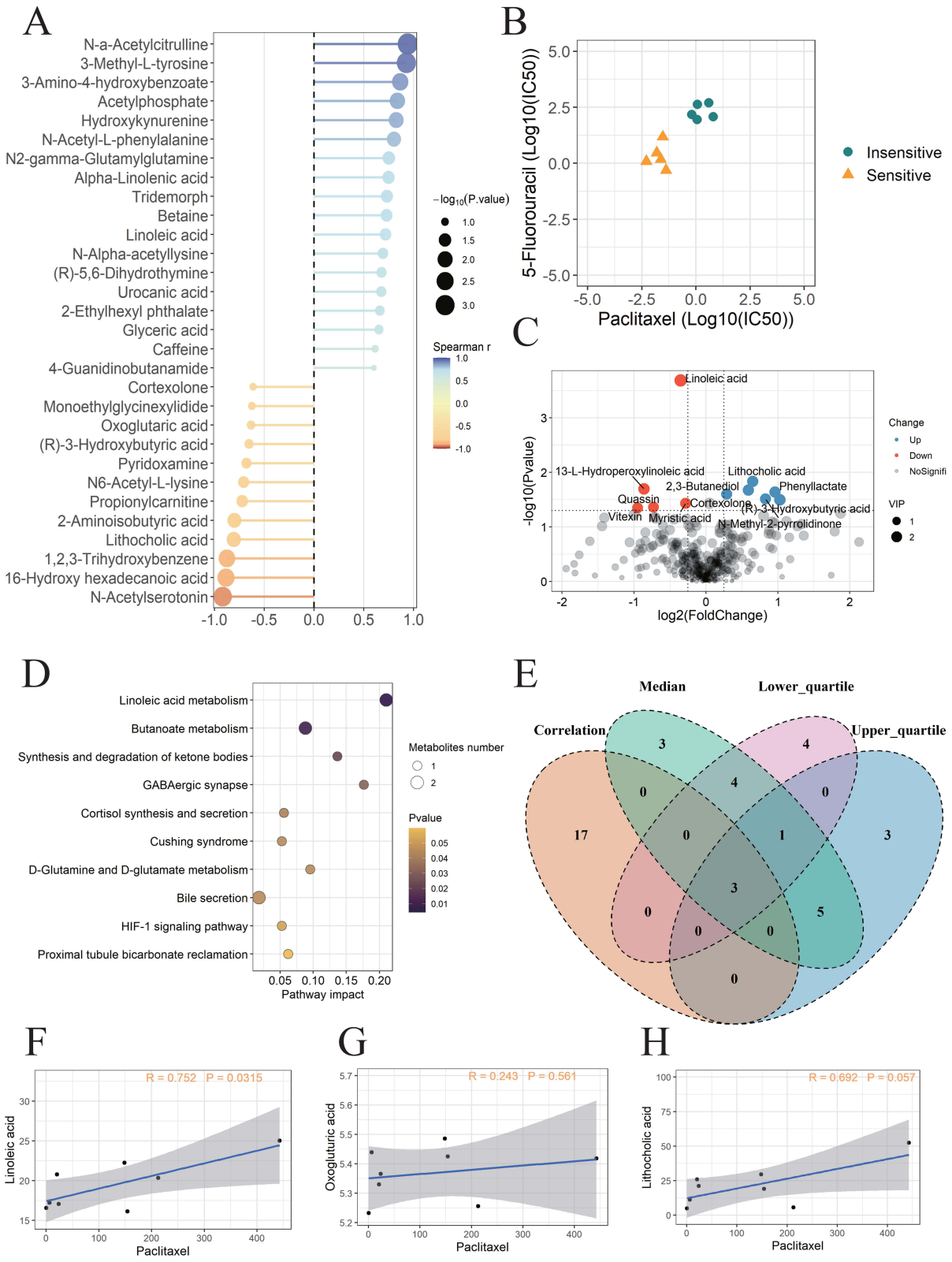

Figure 4 Metabolomics analysis of Paclitaxel drug sensitivity. (**A**) Bubble plot summarizing the top 30 serum metabolites showing the strongest associations with paclitaxel response across organoids. (**B**) Scatter plot of drug sensitivity, with the x-axis representing Paclitaxel Log10 (IC50) and the y-axis representing 5-fluorouracil Log10 (IC50) (n=10, Insensitive=5, Sensitive=5). (**C**) Volcano plot showing differential metabolites. (**D**) Bubble plot of KEGG pathway enrichment analysis. (**E**) Venn diagram integrating results from multiple complementary analyses. (**F**–**H**) Correlations between Paclitaxel IC50 values and the levels of lithocholic acid (**F**) (n=8), oxoglutaric acid (**G**) (n=8), and linoleic acid (**H**) (n=8).

https://doi.org/10.2147/DDDT.S577058

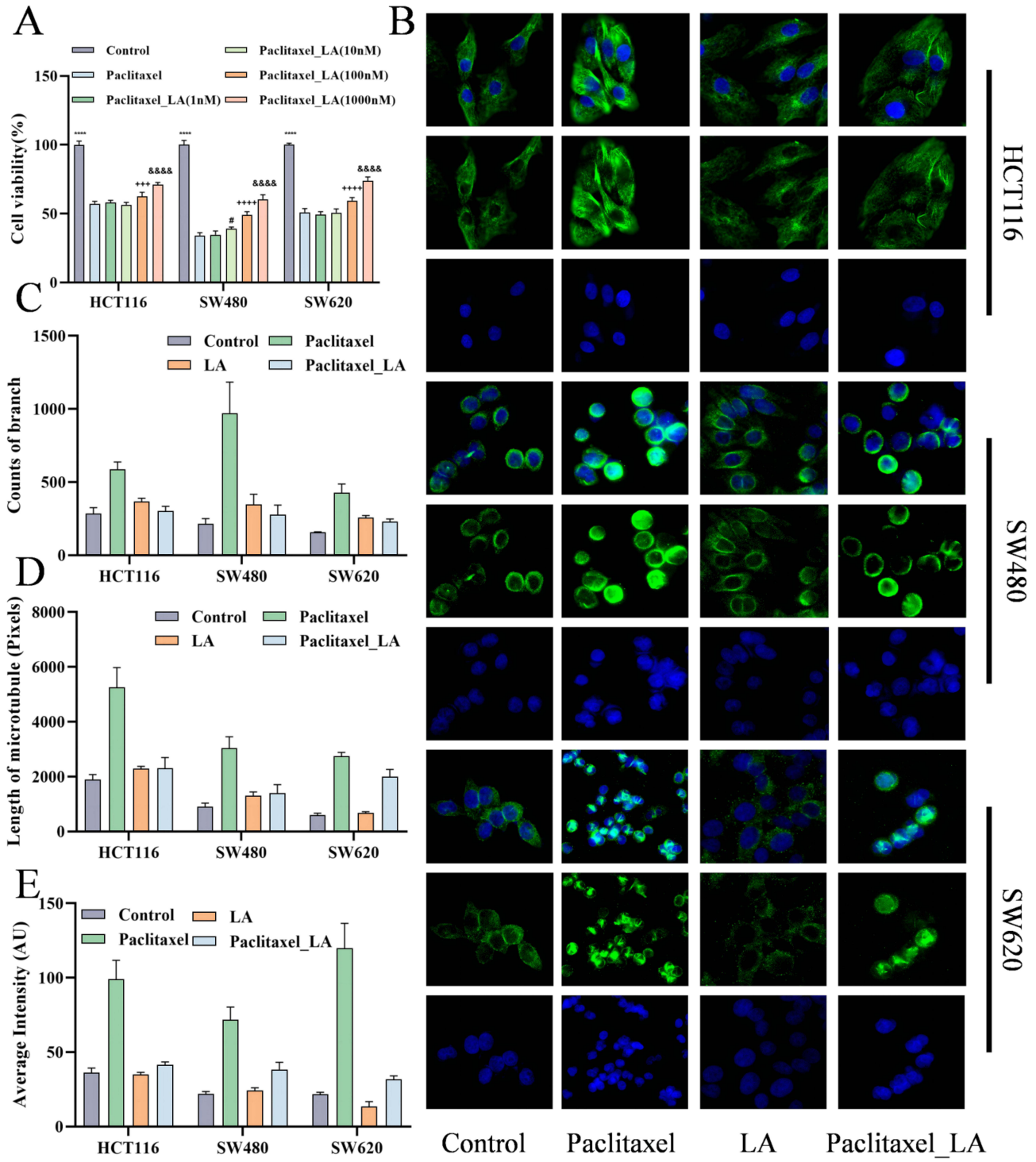

Figure 5 Effect of paclitaxel and linoleic acid on cellular microtubules. Cells were treated with 22nM paclitaxel with or without linoleic acid (1000nM). (**A**) Cell survival rate of different administration groups (n=6). Data are represented as mean ± SD. ****p<0.0001, Control vs Paclitaxel; #p<0.005, Paclitaxel_LA(10nM) vs Paclitaxel; +++p<0.001, ++++p<0.0001 Paclitaxel_LA(100nM) vs Paclitaxel; &&&&p<0.0001 Paclitaxel_LA(1000nM) vs Paclitaxel. (**B**) Immunofluorescence images of microtubules (n=3). (**C**) Counts of branches (n=3). (**D**) Length of microtubule (n=3). (**E**) Average fluorescence intensity (n=3). Data are represented as mean ± SD. These analyses are exploratory (n=3). Results are presented as bootstrap 95% confidence intervals (10000 resamples), without formal hypothesis testing.

across the cell lines. The bootstrap confidence intervals are recorded in Table S5. LA by itself induced only modest microtubule elongation. Notably, co-treatment with LA was associated with reduced Paclitaxel-driven increases in intensity, branching, and length. Together, these results show that LA attenuates Paclitaxel-induced microtubule stabilization and thereby limits the drug's cytotoxicity in colorectal cancer cells.

Effect of Paclitaxel and Linoleic Acid on the Cell Cycle

As shown in Figure 6, paclitaxel alone caused marked G2/M accumulation in HCT116 and SW480 cells, whereas SW620 cells were arrested in S/G2. These patterns reflect a strong mitotic blockade driven by microtubule stabilization and sustained spindle-assembly–checkpoint activation. The bootstrap confidence intervals are recorded in Table S6. LA monotherapy slightly reduced the G1 fraction and increased the proportions in S and G2/M, but its effects were far weaker than those of paclitaxel. Strikingly, co-treatment with LA substantially relieved the drug-induced arrest. Together, these results indicate that LA disrupts paclitaxel-mediated microtubule stabilization, dampens spindle-checkpoint activation, and thereby mitigates the resultant cell-cycle blockade, allowing partial progression through the cycle.

Effect of Linoleic Acid on Paclitaxel in vivo

To further validate the findings from cell-based assays, we established a CT26 tumor-bearing mouse model. No mortality occurred in any group during the 21-day experimental period, and all mice remained alive until the experimental endpoint. The endpoint was defined as day 21, when the largest tumor in the model group reached approximately 2000 mm^3, in accordance with humane criteria, and mice were humanely euthanized for sample collection (Figure 7A). Body weight increased steadily across groups, with a significant difference observed only between the paclitaxel and linoleic acid groups at day 21 ($p = 0.0249$), indicating that the treatments were generally well tolerated (Figure 7B).

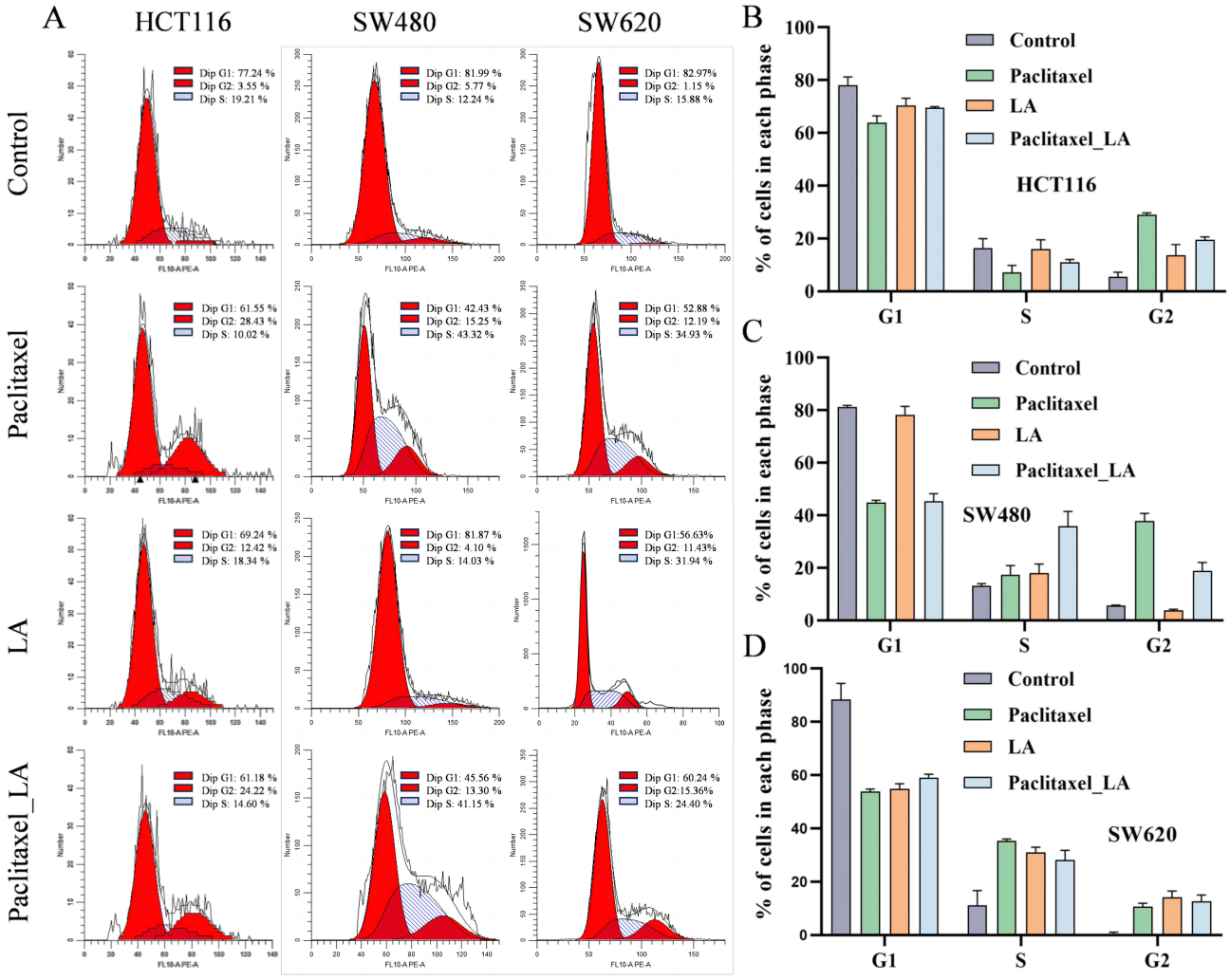

Figure 6 Effect of Paclitaxel and linoleic acid on the cell cycle. Cells were treated with 22nM paclitaxel with or without linoleic acid (1000nM). (**A**) Representative image of cell cycle analysis by flow cytometry (n=3). (**B-D**) Relative percentages of cells per cycle in different treatment groups (n=3). (**B**) HCT116, (**C**) SW480, (**D**) SW620. Data are represented as mean ± SD. These analyses are exploratory (n=3). Results are presented as bootstrap 95% confidence intervals (10000 resamples), without formal hypothesis testing.

https://doi.org/10.2147/DDDT.S577058

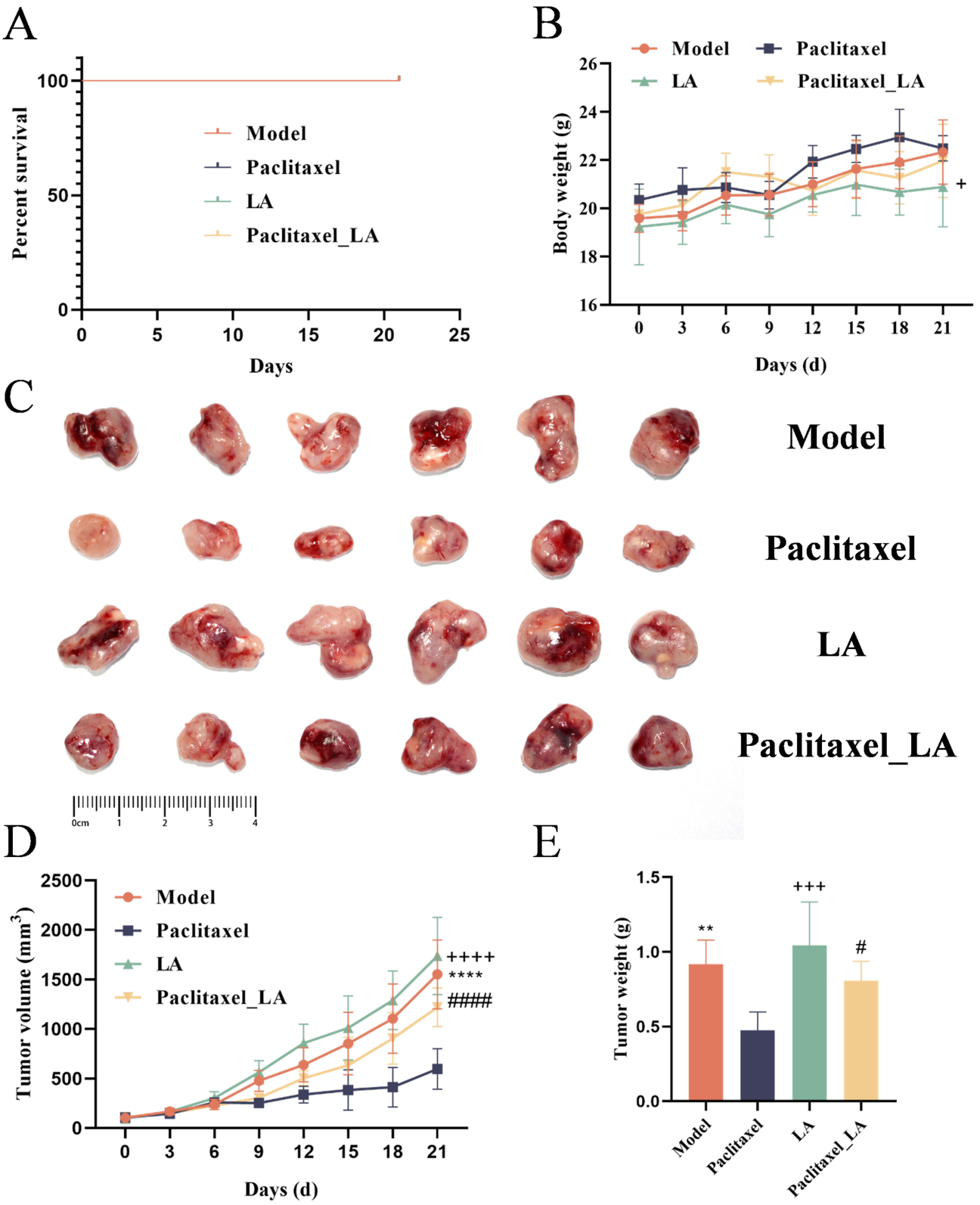

Figure 7 Effects of paclitaxel and linoleic acid on tumor growth in CT26 tumor-bearing mice. (**A**) Kaplan–Meier survival curve showing that no mortality occurred in any group during the 21-day experimental period (n=6). (**B**) Body weight changes of mice during treatment (n=6). (**C**) Representative tumor images from each group at the endpoint (n=6). (**D**) Curves of tumor volume in the model, linoleic acid, paclitaxel and combination groups (n=6). (**E**) Tumor weights in the model, linoleic acid, paclitaxel and combination groups (n=6). Data are represented as mean ± SD. **p<0.01, ****p<0.0001, Control vs Paclitaxel; +p<0.05, +++p<0.001, ++++p<0.0001, LA vs Paclitaxel; #p<0.05, ####p<0.0001, Paclitaxel_LA vs Paclitaxel.

https://doi.org/10.2147/DDDT.S577058

Representative excised tumors from each group are shown in Figure 7C. Tumor growth analysis demonstrated that paclitaxel alone produced the strongest inhibitory effect on tumor progression. By day 21, tumor volumes in the model, linoleic acid, and combination groups were all significantly greater than those in the paclitaxel group (all $p < 0.0001$; Figure 7D). Longitudinal tumor growth was analyzed using a linear mixed-effects model, revealing a significant group X days interaction ($p < 0.0001$; Supplementary Table S7). Estimated tumor growth rates are shown in Supplementary Table S8, and the comparison results were provided in Supplementary Table S9. Consistently, tumor weights at the endpoint were significantly lower in the paclitaxel group compared with the model ($p = 0.0031$), linoleic acid ($p = 0.0002$), and combination groups ($p = 0.0284$) (Figure 7E) The statistical results are presented in Table S10 and S11. Collectively, these in vivo results corroborated our previous findings: linoleic acid alone exhibited limited antitumor activity, whereas its combination with paclitaxel attenuated the therapeutic efficacy of paclitaxel. These results provide in vivo evidence that linoleic acid interferes with the tumor-suppressive effect of paclitaxel in colorectal cancer.

Discussion

Chemotherapy remains a cornerstone in colorectal cancer management, significantly improving overall survival and quality of life. However, treatment outcomes vary widely among patients, reflecting the complex influence of metabolic reprogramming, genetic regulation, and cell death pathways on therapeutic response.[33–35] Conventional in vivo and in vitro models, including established cell lines, tumor spheres, and xenografts, fail to fully capture the complexity of the tumor microenvironment and often overlook inter-patient metabolic heterogeneity.[36] In contrast, patient-derived tumor organoids (PDTOs) retain the histopathological, molecular, and genomic features of primary tumors, and their ability to recapitulate individualized drug responses has made them powerful platforms for high-throughput chemosensitivity testing and precision therapy design.[37–39] In this study, we leveraged the advantages of colorectal cancer PDTOs to model patient-specific responses and successfully identified linoleic acid as a metabolic factor associated with differential sensitivity to paclitaxel.[40,41]

Consistent with our clinical observations, some colorectal cancer patients who were insensitive to 5-fluorouracil exhibited marked sensitivity to paclitaxel. As a prototypical microtubule-targeting agent, paclitaxel prevents microtubule depolymerization, induces mitotic arrest, and suppresses tumor cell proliferation.[42] Originally developed for breast and ovarian cancers, paclitaxel and related microtubule inhibitors have demonstrated therapeutic potential in colorectal cancer, particularly when combined with chemotherapy or immunotherapy, where they enhance antitumor efficacy.[43,44] However, the clinical utility of paclitaxel in CRC remains limited by pronounced inter-patient variability in drug response and the rapid emergence of resistance, phenomena increasingly linked to metabolic reprogramming and tumor adaptation. These challenges highlight the need for predictive biomarkers that can stratify patients and guide the rational clinical application and future repositioning of paclitaxel in colorectal cancer therapy.

Our metabolomic analyses revealed that serum linoleic acid levels were positively correlated with the IC50 of paclitaxel across patient-derived organoids, colorectal cancer cell lines, and tumor-bearing mouse models, indicating that elevated LA is associated with reduced chemosensitivity. This consistent relationship across multiple experimental systems supports LA as a candidate biomarker associated with paclitaxel response. Mechanistically, increased LA levels may influence membrane composition, drug uptake, or microtubule dynamics, thereby attenuating the cytotoxic effects of microtubule-targeting chemotherapy. From a translational perspective, these findings suggest that serum LA may have potential relevance for patient stratification in future studies of paclitaxel response, although further validation in larger cohorts is required.

In the present study, serum samples were collected under standardized fasting conditions to minimize the influence of acute dietary intake. Nevertheless, interindividual variability in serum LA levels was still observed, suggesting that circulating LA levels may reflect longer-term dietary patterns, lipid metabolic status, or underlying metabolic dysregulation rather than short-term nutritional exposure. Chronic dietary habits, adipose tissue lipid turnover, and alterations in fatty acid metabolism associated with metabolic disorder may all contribute to baseline differences in circulating LA. Importantly, subgroup analyses demonstrated that paclitaxel sensitivity was not significantly associated with common clinical characteristics, including BMI, age, sex, or stage. It could also be due to the limitations of the sample size. These findings indicate that variability in chemotherapeutic response cannot be fully explained by routine

demographic or disease-related factors alone, highlighting the potential relevance of metabolic context in shaping treatment sensitivity.

Paclitaxel exerts its antitumor effects by binding to β-tubulin, stabilizing microtubules, and preventing their depolymerization, thereby inducing mitotic arrest and apoptosis in cancer cells. Linoleic acid, an abundant component of membrane phospholipids, can alter membrane biophysical properties such as fluidity and curvature, which in turn influence cytoskeletal organization and microtubule dynamics.[45] Previous studies have shown that elevated linoleic acid levels promote dynamic remodeling of microtubules, increasing their flexibility and turnover.[46] Such alterations may counteract the stabilizing effects of paclitaxel, diminishing its ability to induce mitotic arrest and thereby reducing chemosensitivity. Moreover, changes in membrane composition could also affect drug uptake or intracellular distribution, further modulating therapeutic efficacy. Together, these findings suggest that metabolic states, particularly lipid composition, can regulate chemotherapy response by reshaping the cellular environment in which microtubule-targeting agents exert their function. Rather than acute dietary manipulation, which may have limited and variable effects, strategies aimed at modulating long-term lipid metabolism or membrane–cytoskeleton interactions may represent more feasible approaches to counteract LA-associated chemoresistance. Potential avenues include metabolic interventions that alter fatty acid handling, pharmacological modulation of lipid synthesis or remodeling pathways, and rational combination strategies targeting both microtubule dynamics and lipid–membrane homeostasis. Although these concepts remain speculative and were not directly tested in the current study, they provide a framework for future investigations exploring how metabolic profiling could inform personalized therapeutic strategies and optimize chemotherapeutic efficacy.

Conclusion

In conclusion, this study identifies linoleic acid (LA) as a candidate metabolic biomarker associated with paclitaxel sensitivity in colorectal cancer. Serum LA may have potential relevance for patient stratification and individualized therapeutic decision-making, particularly in cases of conventional chemotherapy resistance. Future investigations focusing on metabolic modulation or combination strategies may further improve our understanding of the mechanisms underlying variability in response to microtubule-targeting agents such as paclitaxel in colorectal cancer. A limitation of this study is the relatively small size of the metabolomics validation cohort. Although consistent associations were observed across PDOs, cell lines, and in vivo models, future studies with larger independent cohorts will be required to further validate the clinical generalizability of these findings. In addition, tumor volume measurements and image quantification were not performed under blinded conditions, which may introduce potential measurement bias in quantitative endpoints.

Abbreviations

CRC, Colorectal Cancer; PDTO, Patient-Derived Tumor Organoid; 5-FU, 5-Fluorouracil; WES, Whole Exome Sequencing; HE, Hematoxylin and Eosin; IHC, Immunohistochemistry; SMA, Smooth Muscle Actin; CK20, Cytokeratin 20; DAPI, 4′,6-Diamidino-2-Phenylindole; PBS, Phosphate-Buffered Saline; DMEM/F12, Dulbecco's Modified Eagle Medium/Nutrient Mixture F-12; CO_2, Carbon Dioxide; DMSO, Dimethyl Sulfoxide; CCK-8, Cell Counting Kit-8; IC_{50}, Half Maximal Inhibitory Concentration; PCA, Principal Component Analysis; KEGG, Kyoto Encyclopedia of Genes and Genomes; CNV, Copy Number Variation; SNV, Single Nucleotide Variant; InDel, Insertion/Deletion; ESI, Electrospray Ionization; HCD, Higher-energy Collisional Dissociation; QC, Quality Control; RSD, Relative Standard Deviation.

Ethics Approval and Informed Consent

This study adheres to the national guidelines and has received approval from the Nanjing Hospital of Chinese Medicine affiliated to Nanjing University of Chinese Medicine Ethics Committee (Approval No.: KY2022309).

Acknowledgments

The authors express their gratitude to all the patients who generously donated their specimens and took part in this study.

Author Contributions

Bingwen Zhou: Validatioin, Visualization Writing – review & editing, Formal analysis. Jinjin Pan: Writing – Original Draft, Writing – review & editing. Mengjie Wang: Methodology, Validation. Peng Zhou: Resources. Zhili Li: Resources. Jingwei Cui: Data Curation. Chuyue Huang: Formal analysis. Lu Wang: Supervision, Project administration. Zhimin Fan: Conceptualization, Supervision, Funding acquisition.

Funding

Jiangsu Key Research and Development Program (Social Development) Project (BE2021611); Scientific research project of Jiangsu Association of Traditional Chinese Medicine (CYTF2024020); Jiangsu Province Youth Science and Technology Talent Support Program (JSTJ-20250220).

Disclosure

The author(s) report no conflicts of interest in this work.

References

1. Zhu M, Zhang P, Yu S, et al. Targeting ZFP64/GAL-1 axis promotes therapeutic effect of nab-Paclitaxel and reverses immunosuppressive microenvironment in gastric cancer. *J Exp Clin Cancer Res*. 2022;41(1):14. doi:10.1186/s13046-021-02224-x
2. Guo C, Zhang W, Zhang Q, et al. Novel dual CAFs and tumour cell targeting pH and ROS dual sensitive micelles for targeting delivery of Paclitaxel to liver cancer. *Artif Cells Nanomed Biotechnol*. 2023;51(1):170–179. doi:10.1080/21691401.2023.2193221
3. Francis PA, Kris MG, Rigas JR, Grant SC, Miller VA. Paclitaxel (Taxol) and docetaxel (Taxotere): active chemotherapeutic agents in lung cancer. *Lung Cancer*. 1995;12(Suppl 1):S163–72. doi:10.1016/0169-5002(95)00432-z
4. Scribano CM, Wan J, Esbona K, et al. Chromosomal instability sensitizes patient breast tumors to multipolar divisions induced by Paclitaxel. *Sci Transl Med*. 2021;13(610):eabd4811. doi:10.1126/scitranslmed.abd4811
5. Wang Y, Zhang C, Zhang S, et al. Kanglaite sensitizes colorectal cancer cells to Paclitaxel via NF-κB inhibition and connexin 43 upregulation. *Sci Rep*. 2017;7(1):1280. doi:10.1038/s41598-017-01480-2
6. Brognard J, Dennis PA. Variable apoptotic response of NSCLC cells to inhibition of the MEK/ERK pathway by small molecules or dominant negative mutants. *Cell Death Differ*. 2002;9(9):893–904. doi:10.1038/sj.cdd.4401054
7. Murphy CC, Harlan LC, Warren JL, Geiger AM. Race and insurance differences in the receipt of adjuvant chemotherapy among patients with stage III colon cancer. *J Clin Oncol*. 2015;33(23):2530–2536. doi:10.1200/JCO.2015.61.3026
8. Vennin C, Cattaneo CM, Bosch L, et al. Taxanes trigger cancer cell killing in vivo by inducing non-canonical T cell cytotoxicity. *Cancer Cell*. 2023;41(6):1170–1185.e12. doi:10.1016/j.ccell.2023.05.009
9. Hejazi M, Baghbani E, Amini M, et al. MicroRNA-193a and paclitaxel combination: a new strategy for treatment of colorectal cancer. *J Cell Biochem*. 2020;121(2):1388–1399. doi:10.1002/jcb.29374
10. Zhang QQ, Wu XJ, Tang T, et al. Quantitative analysis of rectal cancer by spectral domain optical coherence tomography. *Phys Med Biol*. 2012;57(16):5235–5244. doi:10.1088/0031-9155/57/16/5235
11. Tang Y, Wang T, Hu Y, et al. Cutoff value of IC(50) for drug sensitivity in patient-derived tumor organoids in colorectal cancer. *iScience*. 2023;26(7):107116. doi:10.1016/j.isci.2023.107116
12. Patel SG, May FP, Anderson JC, et al. Updates on age to start and stop colorectal cancer screening: recommendations from the U.S. Multi-Society Task Force on Colorectal Cancer. *Gastroenterology*. 2022;162(1):285–299. doi:10.1053/j.gastro.2021.10.007
13. Jin H, Cheng X, Nguyen N, et al. Abstract 815: using CRISPR/Cas9 to generate isogenic cell lines and reference standards for applications in cancer diagnostics. *Cancer Res*. 2017;77(13_Supplement):815. doi:10.1158/1538-7445.AM2017-815
14. Li M, Izpisua Belmonte JC. Organoids – preclinical models of human disease. *N Engl J Med*. 2019;380(6):569–579. doi:10.1056/NEJMra1806175
15. Ma X, Wang Q, Li G, Li H, Xu S, Pang D. Cancer organoids: a platform in basic and translational research. *Genes Dis*. 2023;11(2):614–632. doi:10.1016/j.gendis.2023.02.052
16. Cartry J, Bedja S, Boilève A, et al. Implementing patient derived organoids in functional precision medicine for patients with advanced colorectal cancer. *J Exp Clin Cancer Res*. 2023;42(1):281. doi:10.1186/s13046-023-02853-4
17. He X, Jiang Y, Zhang L, et al. Patient-derived organoids as a platform for drug screening in metastatic colorectal cancer. *Front Bioeng Biotechnol*. 2023;11:1190637. doi:10.3389/fbioe.2023.1190637
18. Ooft SN, Weeber F, Dijkstra KK, et al. Patient-derived organoids can predict response to chemotherapy in metastatic colorectal cancer patients. *Sci Transl Med*. 2019;11(513):eaay2574. doi:10.1126/scitranslmed.aay2574
19. Mo S, Tang P, Luo W, et al. Patient-derived organoids from colorectal cancer with paired liver metastasis reveal tumor heterogeneity and predict response to chemotherapy. *Adv Sci*. 2022;9(31):e2204097. doi:10.1002/advs.202204097
20. Pasch CA, Favreau PF, Yueh AE, et al. Patient-derived cancer organoid cultures to predict sensitivity to chemotherapy and radiation. *Clin Cancer Res*. 2019;25(17):5376–5387. doi:10.1158/1078-0432.CCR-18-3590
21. Yao Y, Xu X, Yang L, et al. Patient-derived organoids predict chemoradiation responses of locally advanced rectal cancer. *Cell Stem Cell*. 2020;26(1):17–26.e6. doi:10.1016/j.stem.2019.10.010
22. Drost J, Clevers H. Organoids in cancer research. *Nat Rev Cancer*. 2018;18(7):407–418. doi:10.1038/s41568-018-0007-6
23. Terry AR, Hay N. Emerging targets in lipid metabolism for cancer therapy. *Trends Pharmacol Sci*. 2024;45(6):537–551. doi:10.1016/j.tips.2024.04.007
24. Qin J, Ye L, Wen X. Fatty acids in cancer chemoresistance. *Cancer Lett*. 2023;572:216352. doi:10.1016/j.canlet.2023.216352

25. Atashi N, Eshaghian N, Anjom-Shoae J, et al. Dietary intake and tissue biomarkers of omega-6 fatty acids and risk of colorectal cancer in adults: a systematic review and dose-response meta-analysis of prospective cohort studies. *Nutr Diabetes*. 2025;15(1):17. doi:10.1038/s41387-025-00367-w
26. Wang Z, Wang Y, Li Z. Lipid metabolism as a target for cancer drug resistance: progress and prospects. *Front Pharmacol*. 2023;14:1274335. doi:10.3389/fphar.2023.1274335
27. Mangaonkar S, Nath S, Chatterji BP. Microtubule dynamics in cancer metastasis: harnessing the underappreciated potential for therapeutic interventions. *Pharmacol Ther*. 2024;263:108726. doi:10.1016/j.pharmthera.2024.108726
28. Zhang Y, Ye L, Qin Y. Serum metabolomics to identify molecular subtypes and predict XELOX efficacy in colorectal cancer. *Sci Rep*. 2025;15(1):13671. doi:10.1038/s41598-025-97463-9
29. Costantini S, Gennaro ED, Capone F. Plasma metabolomics, lipidomics and cytokinomics profiling predict disease recurrence in metastatic colorectal cancer patients undergoing liver resection. *Front Oncol*. 2023;12:1110104. doi:10.3389/fonc.2022.1110104
30. Yuan F, Jia G, Wen W. Blood metabolic biomarkers and colorectal cancer risk: results from large prospective cohort and Mendelian randomization analyses. *Br J Cancer*. 2025;133(1):94–103. doi:10.1038/s41416-025-02997-4
31. Phan N, Hong JJ, Tofig B, et al. A simple high-throughput approach identifies actionable drug sensitivities in patient-derived tumor organoids. *Commun Biol*. 2019;2:78. doi:10.1038/s42003-019-0305-x
32. LeSavage BL, Suhar RA, Broguiere N, Lutolf MP, Heilshorn SC. Next-generation cancer organoids. *Nat Mater*. 2022;21(2):143–159. doi:10.1038/s41563-021-01057-5
33. Zhang J, Zou S, Fang L. Metabolic reprogramming in colorectal cancer: regulatory networks and therapy. *Cell Biosci*. 2023;13(1):25. doi:10.1186/s13578-023-00977-w
34. Yang C, Huang S, Cao F, Zheng Y. A lipid metabolism-related genes prognosis biomarker associated with the tumor immune microenvironment in colorectal carcinoma. *BMC Cancer*. 2021;21(1):1182. doi:10.1186/s12885-021-08902-5
35. Schiliro C, Firestein BL. Mechanisms of metabolic reprogramming in cancer cells supporting enhanced growth and proliferation. *Cells*. 2021;10(5):1056. doi:10.3390/cells10051056
36. Katt ME, Placone AL, Wong AD, Xu ZS, Searson PC. In vitro tumor models: advantages, disadvantages, variables, and selecting the right platform. *Front Bioeng Biotechnol*. 2016;4:12. doi:10.3389/fbioe.2016.00012
37. Tuveson D, Clevers H. Cancer modeling meets human organoid technology. *Science*. 2019;364(6444):952–955. doi:10.1126/science.aaw6985
38. Broutier L, Mastrogiovanni G, Verstegen MM, et al. Human primary liver cancer-derived organoid cultures for disease modeling and drug screening. *Nat Med*. 2017;23(12):1424–1435. doi:10.1038/nm.4438
39. Vlachogiannis G, Hedayat S, Vatsiou A, et al. Patient-derived organoids model treatment response of metastatic gastrointestinal cancers. *Science*. 2018;359(6378):920–926. doi:10.1126/science.aao2774
40. Seidlitz T, Merker SR, Rothe A, et al. Human gastric cancer modelling using organoids. *Gut*. 2019;68(2):207–217. doi:10.1136/gutjnl-2017-314549
41. Vivarelli S, Candido S, Caruso G, Falzone L, Libra M. Patient-derived tumor organoids for drug repositioning in cancer care: a promising approach in the era of tailored treatment. *Cancers*. 2020;12(12):3636. doi:10.3390/cancers12123636
42. Albahde MAH, Abdrakhimov B, Li GQ, et al. The role of microtubules in pancreatic cancer: therapeutic progress. *Front Oncol*. 2021;11:640863. doi:10.3389/fonc.2021.640863
43. Murono K, Nagata H, Ishimaru K, et al. Safety of intraperitoneal Paclitaxel combined with conventional chemotherapy for colorectal cancer with peritoneal carcinomatosis: a Phase I trial. *Cancer Chemother Pharmacol*. 2019;83(1):145–150. doi:10.1007/s00280-018-3714-5
44. Kim IW, Yoon AR, Hong J, Kasala D, Yun CO. Synergistic antitumor immune response mediated by Paclitaxel-conjugated nanohybrid oncolytic adenovirus with dendritic cell therapy. *Front Immunol*. 2024;15:1355566. doi:10.3389/fimmu.2024.1355566
45. El-Far SW, Abo El-Enin HA, Abdou EM, Nafea OE, Abdelmonem R. Targeting colorectal cancer cells with niosomes systems loaded with two anticancer drugs models; comparative in vitro and anticancer studies. *Pharmaceuticals*. 2022;15(7):816. doi:10.3390/ph15070816
46. Masner M, Lujea N, Bisbal M, Acosta C, Kunda P. Linoleic and oleic acids enhance cell migration by altering the dynamics of microtubules and the remodeling of the actin cytoskeleton at the leading edge. *Sci Rep*. 2021;11(1):14984. doi:10.1038/s41598-021-94399-8